Fine Chemical Engineering
http://ojs.wiserpub.com/index.php/FCE/

Research Article

Green Synthesis of Sulphuric Acid Based on "Geber's Method": A Detailed Aspen Plus Simulation

Abdulhalim Musa Abubakar[1*], Bukar Lawan[2], Mohamed Saad[3], Luqman Buba Umdagas[2], Azhar Abbas[4], Habib Muhammad Shettima[2], Ronny Mönnig[5], Semiu Adebayo Kareem[1]

[1]Department of Chemical Engineering, Faculty of Engineering, Modibbo Adama University, Yola, Nigeria
[2]Department of Chemical Engineering, Faculty of Engineering, University of Maiduguri, Borno State, Nigeria
[3]Chemical Engineering Department, Sirte University, Sirte, Libya
[4]Department of Chemical Engineering, MNS University of Engineering and Technology, Multan, Pakistan
[5]Department of System Calibration, Business Area Future Powertrain, IAV, GmbH, Berlin, Germany
E-mail: abdulhalim@mau.edu.ng

Received: 20 June 2024; **Revised:** 27 August 2024; **Accepted:** 12 September 2024

Graphical abstract:

Geber's method sulphuric acid synthesis route

Abstract: Sulfuric acid (H_2SO_4) has a wide range of applications, but its current synthesis route via the contact process negatively impacts the atmospheric environment with harmful gaseous pollutants. Thus, based on the non-random two-liquids (NRTL) thermodynamic method, this study presents a detailed Aspen Plus V8.8 simulation of the green synthesis route of H_2SO_4 based on Geber's method developed already in the 18th century. The research investigates the efficiency and energy dynamics of the process through the analysis of key process parameters such as reactor's heat

DOI: https://doi.org/10.37256/fce.5220245172

duty, vapor fraction, and molar extent of reaction in the selected configuration, using green vitriol ($FeSO_4 \cdot 7H_2O$) as a natural raw material. This study presented a novel manufacturing route that resulted in H_2SO_4 of 85.76% purity (33.71 kg/h), considering the chosen parameter space. The results highlight the impact of reactant component molar yield and fractional conversion of iron (II) sulfate ($FeSO_4$) on heat duty and the optimal molar extent for maximizing H_2SO_4 production in a series of equilibrium reactors. In addition, appropriate operational parameters for the synthesis process were carefully specified, offering a pathway towards sustainable and eco-friendly H_2SO_4 production, which should emit zero greenhouse gases. Further optimization of the reactor conditions, can help maximize the yield of H_2SO_4, while minimizing energy consumption and byproduct formation. Developing advanced wastewater treatment units to purify the wastewater stream containing trace amounts of H_2SO_4 and dissolved sulfur trioxide (SO_3) can mitigate environmental impact and ensure compliance with regulatory standards.

***Keywords*:** sulphuric acid, green vitriol, Geber's method, ferrous sulfate, sulfur trioxide, Aspen Plus simulation

1. Introduction

The synthesis of sulfuric acid (H_2SO_4) is a critical industrial process with wide-ranging applications in chemical manufacturing, fertilizer production, petroleum refining, and wastewater processing. Traditionally, the production of H_2SO_4 has relied on the contact process, which, while highly efficient, involves significant energy consumption and toxic materials usage, leading to environmental concerns. Because, in the industrial manufacture of H_2SO_4, about 60% of the sulfur dioxide (SO_2) originates from sulfur burning and about 40% comes from roasting sulfur minerals.[1-2] The quest for more sustainable and eco-friendly methods has driven researchers to explore green chemistry approaches, including possibilities for recycling. One such approach revisits the historical "Geber's Method", a process attributed to the 18th-century alchemist Jabir ibn Hayyan (Geber), renowned for his contributions to early chemical science.[3] Geber employed green vitriol or melanterite ($FeSO_4 \cdot 7H_2O$-ferrous sulfate heptahydrate) to synthesize H_2SO_4. Prominent examples of other acids that can be synthesized using green vitriol are hydrochloric acid, nitric acid, and sulfurous acid (H_2SO_3). Amongst the list, nitric acid preparation from green vitriol dates back to the work of German chemist Johann Rudolf Glauber in the 17th century.[4] Recent advancements in green chemistry have sparked renewed interest in developing H_2SO_4 production methods that minimize environmental impact. Contemporary research has primarily focused on optimizing the contact process to reduce emissions and improve energy efficiency.[5-6] Infoplease mentioned that the process was developed by Peregrine Phillips in England in 1831.[7] Studies have also explored alternative raw materials and catalytic methods to lower the carbon footprint of H_2SO_4 production. However, these approaches rely on significant energy inputs and complex, costly infrastructure.

Despite these efforts, there remains a notable research gap in the comprehensive modeling and simulation of green synthesis methods using modern engineering tools. Though the void is not total,[8-9] the potential of employing Aspen Plus, a robust process simulation software, to optimize and validate eco-friendly production methods has not been thoroughly investigated, according to our best knowledge. This study aims to fill this gap by conducting a detailed Aspen Plus simulation of H_2SO_4 synthesis based on Geber's method. By taking advantage of Aspen Plus sophisticated feature, we aim to model the entire process, analyze its feasibility, and identify optimization opportunities for a greener, more sustainable production method. In this context, our research not only revisits a historical technique with modern tools but also contributes to the ongoing efforts in green chemistry to develop sustainable industrial processes. Through this simulation, a potential pathway for the industrial adoption of a greener H_2SO_4 synthesis technique is presented. Moreso, via the detailed analysis of reactor performance and phase behavior, the study advances the understanding of the thermodynamic parameters involved in the green synthesis of H_2SO_4 using Geber's method. The study further emphasizes the importance of recycling byproducts and minimizing waste generation, to promote environmentally friendly and sustainable chemical manufacturing practices. It also eliminates the need for a catalyst that reduces SO_2 emissions in conventional processes, as researched by Richardson et al.[10] A study carried out by Mohammed et al.[11] additionally lowers SO_2 emission using a counter-current stream of sodium hydroxide (NaOH) solution in a bench-scale system. Only rigorous analysis can pinpoint the finest industry approach peculiar to the desire of each H_2SO_4 manufacturing plant that may be sited. However, looking at the prevailing detrimental impact caused by H_2SO_4 plant

emission into the air,[12] the best option should be the one with the lowest-to-zero SO_2 and/or SO_3 release. For instance, Worley reported 95% SO_2 emission reduction based on the Chemetics' CORE-SO_2^{TM} technology implemented for the Arafura H_2SO_4 plant in Australia's Northern Territory.[13] Lemessa et al. simulated the reduction of SO_2 down to 0.12 mol% for the Awash Melkassa Aluminum Sulfate and Sulfuric Acid Share Company (AMASSASC) in Addis Ababa, Ethiopia, using Aspen Hysys.[14] An ever-increasing H_2SO_4 output volume projected to be about 294.67 million metric tons in 2026, will only exacerbate the current emission challenges if adequate measures are not put in place.[15]

2. Methodology

2.1 *Components property*

Components of specific interest in the simulation of H_2SO_4 manufacture are listed in Table 1 together with some of their important chemical properties. These properties were used to guide the selection of valid phases in all units under consideration, as well as enhance the appropriate specification of stream and block conditions necessary to run the process.

Table 1. Participating components and their physical and chemical properties

Compound	Formula	Molecular weight 'MW' (g/mol)	Boiling point (°C)	Solubility	Form
Iron (II) sulfate	$FeSO_4$	151.905	300	328 g/L	White crystals
Ferrous sulfate monohydrate	$FeSO_4 \cdot H_2O$	169.9	300	44.69 g/100 mL at 77 °C	White-yellow crystals
Ferrous sulfate tetrahydrate	$FeSO_4 \cdot 4H_2O$	223.9	300	38 g/100 mL	Blue-green monoclinic crystals
Ferrous sulfate heptahydrate	$FeSO_4 \cdot 7H_2O$	278.06	300	51.35 g/100 mL at 54 °C	Blue-green deliquescent crystals
Water/Steam	H_2O	18.02	100	-	Liquid, vapor and ice
Sulfur trioxide	SO_3	80.066	44.75	-	Colorless liquid, ice- or fiber-like crystals & gas
Oxygen	O_2	31.9	-182.962	9.1 mg/L at 20 °C	Colorless & odorless gas
Sulfuric acid	H_2SO_4	98.07	336.85	Miscible with water	Colorless oily liquid
Iron (III) oxide	Fe_2O_3	159.06	3,414	-	Red-brown solid

Note that copperas and/or szomolnokite are other nomenclatures for $FeSO_4 \cdot H_2O$, while $FeSO_4 \cdot 4H_2O$ is termed rozenite.[16] Hematite, ferric oxide and/or red iron oxide are alternative names for Fe_2O_3. For convenience, the abbreviated form of these names was used in this study to identify some streams in the Aspen Plus simulation window. As shown in Table 1, $FeSO_4 \cdot H_2O$, $FeSO_4 \cdot 4H_2O$ and $FeSO_4 \cdot 7H_2O$ whose solubilities are reported for different temperatures,[17] begin to decompose at temperatures > 300 °C (572 °F). It is more appropriate to discuss their decomposition temperature rather than their water of crystallization. Nevertheless, their water of crystallization is lost at around 70-80 °C. Also, as reported by Zhang et al., Fe_2O_3 is insoluble in water. Because SO_3 reacts completely and rapidly with H_2O, it is not typically described in terms of solubility in H_2O in the conventional sense.[18] Instead, it is considered to dissolve by reacting to form H_2SO_4.[19-20]

2.2 *Choosing a thermodynamic property method*

Aspen Plus V8.8 was opened and 'Specialty Chemicals with Metric Units' was chosen under 'Chemical Processes'.

Compound chemicals involved in the synthesis of H_2SO_4 were selected, as shown in Table 1 before executing the properties analysis run. Non-random two-liquids (NRTL) were chosen as the base method for the process after studying its usage described by Vetere[21] and Labarta et al.[22] Then, the ASME 1967 steam table (STEAM-TA) correlation for the free-water method was selected due to its robustness, reliability, comprehensive data, broad applicability, thermodynamic accuracy and consistency with industry standards. De Tommaso et al. mentioned that, when users master the theoretical background, they lessen common mistakes such as the application of an unfitting thermodynamic method, the selection of improper algorithms in the case of tear systems, and the setting of illogical system specifications.[23]

2.3 *Geber's method simulation*

For ease of reference, this study divides the method into two: that is, the decomposition reaction steps (DRS) and SO_3 mixing with water (SO_3H_2O). DRS also consists of two reaction stages, which are dehydration and thermal decomposition in air (TDA).

2.3.1 *Dehydration stage*

Here, green vitriol loses its water of crystallization ($7H_2O$) in the form of vapor, upon heating in accordance with the Reaction 1 pathway.[24]

$$FeSO_4 \cdot 7H_2O_{(s)} \rightarrow FeSO_{4(s)} + 7H_2O_{(g)} \quad (1)$$

However, the loss of '$7H_2O$ or 7 moles of H_2O' occurred following three reaction steps (Reaction 2-4) that were modeled in Aspen Plus using the RYIELD units arranged in series,[25-26] where each reactor was instigated to remove a specific amount of water.

$$FeSO_4 \cdot 7H_2O_{(s)} \rightarrow FeSO_4 \cdot 4H_2O_{(s)} + 3H_2O_{(g)} \quad (2)$$

$$FeSO_4 \cdot 4H_2O_{(s)} \rightarrow FeSO_4 \cdot H_2O_{(s)} + 3H_2O_{(g)} \quad (3)$$

$$FeSO_4 \cdot H_2O_{(s)} \rightarrow FeSO_{4\,(s)} + H_2O_{(g)} \quad (4)$$

Hongbo et al. described a novel procedure for dewatering green vitriol, but it is not quite prominent.[27] In this particular step, Reaction 2 was modeled in the simulation flowsheet window by feeding a 100 kg/h pure stream of $FeSO_4 \cdot 7H_2O$ (basis) to an RYIELD-A reactor. The 'FES-$7H_2O$' feed stream conditions specified were 1 atm pressure and 25 °C temperature, while the unit was set at 1 atm and 70 °C under the 'Specification' tab for the block. In both this work and in Tsiura et al.[16] who employed a temperature of 62 °C, both specifications were within or closer to the usual 70-100 °C for Reaction 2. Such reactor type requires prior knowledge of the reaction stoichiometry and conversion. Under the 'Yield' tab, the two-product component yield per unit mass of the reactant, ejected as a single stream called 'ROZN + H_2O', was calculated and entered on a mole basis. First, moles (n) of the reactant are computed using its MW by applying Equation 1 (E1).

$$n_{FeSO_4 \cdot 7H_2O} = \frac{100\ kg/h}{278.06\ g/mol} = \frac{100{,}000\ g/h}{278.06\ g/mol} = 359.634\ mol/h \quad (E1)$$

Since according to Reaction 2, 1 mol $FeSO_4 \cdot 7H_2O$ produces 1 mol $FeSO_4 \cdot 4H_2O$ and 3 mol H_2O, for 359.634 mol/h of $FeSO_4 \cdot 7H_2O$, the moles of the products would be 359.634 mol/h $FeSO_4 \cdot 4H_2O$ and 3 × 359.634 = 1,078.902 mol/h H_2O. On a mass basis, multiply the MW of the product by the mole basis values. It would be (359.634 mol/h) × (223.9 g/mol) = 80,522 g/h = 80.54 kg/h $FeSO_4 \cdot 4H_2O$ and (1,078.902 mol/h) × (18.02 g/mol) = 19,442 g/h = 19.46 kg/h H_2O.

At this stage, the simulation was re-initialized and run. Afterward, a warning message stating that 'RYIELD physical property parameter DHFORM and DHAQFM is missing for $FeSO_4 \cdot 4H_2O$ and $FeSO_4 \cdot 7H_2O$ component' was hinted by Aspen Plus. It further states that the 'absence of this parameter will result in incorrect enthalpy results'. DHFORM is a pure component scalar parameter representing the standard enthalpy of formation, whereas DHAQFM stands for heat of aqueous formation. To rectify this fault, DHFORM or DHAQFM location for $FeSO_4 \cdot 4H_2O$ and $FeSO_4 \cdot 7H_2O$ was accessed by following the steps: 'Properties' window → 'Components' → '$FeSO_4 \cdot 4H_2O$' or '$FeSO_4 \cdot 7H_2O$' → 'Review' button. The DHFORM for $FeSO_4 \cdot 4H_2O$ (-2,131.06 kJ/mol = -509,357 cal/mol) and for $FeSO_4 \cdot 7H_2O$ (-3,017.51 kJ/mol = -721,202 cal/mol) entered, was obtained in Kobylin et al.[28] The simulation was re-run to obtain the product stream outputs. By charging the 'ROZN + H_2O' stream containing the two-product specie into a SEP1 block, Reaction 2 water of crystallization '$3H_2O$' and $FeSO_4 \cdot 4H_2O$ were split into separate streams called '$3H_2OA$' and 'FES-$4H_2O$', respectively. To obtain pure streams of the respective components of the SEP1 product streams, a split fraction of 1 was specified for the 'FES-$4H_2O$' stream.

RYIELD-B unit to model Reaction 3 and RYIELD-C unit to model Reaction 4 was included following the same principle described under RYIELD-A. Respectively, products of RYIELD-B and RYIELD-C were split using SEP2 and SEP3 blocks in the same way. In the same fashion in the foregone, RYIELD-B and RYIELD-C product yield on a mole basis, as shown in Table 2, were calculated and entered into Aspen Plus. Again, DHFORM = -1,245.65 kJ/mol = -297,697 cal/mol for $FeSO_4 \cdot H_2O$ was found in Kobylin et al.[28] and entered in Aspen Plus, to address the issue with calculating enthalpy that resulted from its absence.

Table 2. Units and streams condition

Block	Stream name	Component	Feed/Product specification	Unit condition
RYIELD-A	Inlet: FES-$7H_2O$	$FeSO_4 \cdot 7H_2O$	100 kg/h pure; 25 °C; 1 atm	70 °C; 1 atm
	Outlet: ROZN + H_2O	$FeSO_4 \cdot 4H_2O$ H_2O	359.634 mol/h yield 1,078.902 mol/h yield	
SEP1	Inlet: ROZN + H_2O	$FeSO_4 \cdot 4H_2O$ H_2O	- -	0 atm
	Outlet: FES-$4H_2O$ $3H_2OA$	$FeSO_4 \cdot 4H_2O$ H_2O	Split Fraction = 1 -	-
RYIELD-B	Inlet: FES-$4H_2O$	$FeSO_4 \cdot 4H_2O$	-	70 °C; 1 atm
	Outlet: SZOM + H_2O	$FeSO_4 \cdot H_2O$ H_2O	359.805 mol/h yield 1,079.415 mol/h yield	
SEP2	Inlet: SZOM + H_2O	$FeSO_4 \cdot H_2O$ H_2O	- -	0 atm
	Outlet: FES-H_2O $3H_2OB$	$FeSO_4 \cdot H_2O$ H_2O	Split Fraction = 1 -	-
RYIELD-C	Inlet: FES-H_2O	$FeSO_4 \cdot H_2O$	-	70 °C; 1 atm
	Outlet: FERS + H_2O	$FeSO_4$ H_2O	359.745 mol/h yield 359.745 mol/h yield	
SEP3	Inlet: FERS + H_2O	$FeSO_4$ H_2O	- -	0 atm
	Outlet: FERS H_2OC	$FeSO_4$ H_2O	Split Fraction = 1 -	-

Aspen Plus is expected to normalize the specified yields in the 3 RYIELD reactors-as such, a warning message

is disclosed, despite raising the maximum iteration to 100. Ordinarily, warnings are classified into minor, moderate and critical in Aspen Plus simulation. Since the kind of warning displayed is a moderate type, these warnings were deliberately ignored. Specifying the reactors' product yield on a mass flow basis, would presumably address this issue. Since all water of crystallization was ejected via streams $3H_2OA$, $3H_2OB$ and H_2OC, $FeSO_4$ in stream 'FERS' was fed to the next block to undergo TDA.

2.3.2 *Thermal decomposition in air*

As reported by Gallagher et al.,[29] anhydrous $FeSO_4$ TDA will give SO_3 when reacted with O_2, in accordance with Reaction 5.

$$4FeSO_{4\,(s)} + O_{2\,(g)} \rightarrow 2Fe_2O_{3\,(s)} + 4SO_{3\,(g)} \tag{5}$$

An RSTOIC reactor was selected where $FeSO_4$ from SEP3 together with separate stream of O_2 was fed. To determine the amount of O_2 needed for the reaction in the RSTOIC reactor, stoichiometry based on Reaction 5 was used. Firstly, mass flow of $FeSO_4$ into the RSTOIC block (in g/h) was fetched from the Aspen Plus 'Stream Summary', and together with its MW (151.095 g/mol), the molar flow (which is 359.698 mol/h) was calculated. Secondly, according to Reaction 5, 4 moles of $FeSO_4$ react with 1 mole of O_2. Therefore, the moles of O_2 required = $\frac{1}{4}\times$ moles of $FeSO_4$ = $\frac{1}{4}\times$ 359.698 mol/h = 89.9245 mol/h. Thus, the amount of O_2 to be fed = (89.9245 mol/h) × (31.9 g/mol) = 2,869 g/h = 2.869 kg/h. According to literature, Reaction 5 occurs at 500-800 °C and 1 atm.[26,30] In this study, RSTOIC block and feed condition was equally taken at 600 °C and 1 atm. In addition, Reaction 5 or 'R1' was defined together with their coefficients in Aspen Plus. The intention is to use SO_3 to produce H_2SO_4. As such, we want to maximize the conversion of $FeSO_4$ to SO_3 in the RSTOIC reactor. In this case, a high fractional conversion of $FeSO_4$ of 0.96 was specified and the simulation was re-run. This was the basis for the selection of RSTOIC reactor, simply because the stoichiometry and conversion of the limiting reactant is known.[31] At the same time, the foregone unit completes the DRS stage.

2.3.3 *SO_3 mixing with water*

It is worthy of note that the RSTOIC unit inlet streams are 'O_2-IN' and 'FERS', while its outlet stream is 'FEO + SO_3', which contains Fe_2O_3, O_2 and SO_3. SEP4 block, was employed in the splitting of stream 'FEO + SO_3' into separate streams of Fe_2O_3, O_2 and SO_3. In SEP4, a split fraction of 1 was specified for both 'SO_3' and 'Fe_2O_3' to exit their respective streams. However, the "O_2-OUT" stream contains both $FeSO_4$ and O_2. Based on Reaction 6, SO_3 can be mixed with H_2O to give aqueous H_2SO_4.[8,32-33]

$$SO_{3\,(g)} + H_2O_{(l)} \rightleftharpoons H_2SO_{4\,(aq)} \tag{6}$$

In this simulation, H_2O byproducts of the RYIELD reactors (i.e., $3H_2OA$, $3H_2OB$ & H_2OC) were mixed (using MIXER) to give a single stream of H_2O (H_2OD), to serve as the reactant in Reaction 6. Generally, the reaction between SO_3 and H_2O to form H_2SO_4 is typically very fast and can be assumed to reach equilibrium almost instantly. An equilibrium reactor (REquil) was seen as appropriate to model this behavior.[34] Industrial processes for producing H_2SO_4 from SO_3 and H_2O typically operate at temperatures ranging from 150-200 °C. This range ensures the reaction proceeds efficiently without causing excessive thermal decomposition of products or reactants. S_3H_2O modelling was carried out in REQUIL-A at 2 atm and 150 °C and by defining the reaction set 'R2' together with its coefficients and molar extent of reaction (ξ). The symbol 'ξ' is the number of moles of the limiting reactant that is being converted. Therefore, the limiting reactant is SO_3 since it has fewer moles compared to H_2O. To determine ξ to be specified in REQUIL-A, Equation 2 (E2) was used.[35-37]

$$\xi_{REq1} = \frac{\dot{n}_{SO_3}{}^{out} - \dot{n}_{SO_3}{}^{in}}{-1} = \frac{\left(\dot{n}_{SO_3}{}^{IMP\text{-}H_2OA} + \dot{n}_{SO_3}{}^{H_2SO_4\text{-}A}\right) - \dot{n}_{SO_3}{}^{SO_3}}{-1} \tag{E2}$$

It is expected that the REQUIL-A product should consist of a liquid stream of < 100% pure H_2SO_4 and a vapor stream of impure H_2O (i.e., mixed with a small amount of unreacted SO_3 and H_2SO_4). To further minimize the concentration of SO_3 in the outlet stream, 'IMP-H_2OA' and 'H_2SO_4-A' streams were fed into another REQUIL-B reactor and a new ξ_{REq2} was calculated and entered. A final wastewater stream 'IMP-H_2OB' was discharged and highly pure H_2SO_4 product can then be collected via stream 'H_2SO_4-B'.

2.4 *Sensitivity analysis*

First, sensitivity analysis was conducted on the RYIELD-A, B & C reactors, where specified unit temperature, molar yields of $FeSO_4 \cdot 4H_2O/FeSO_4 \cdot H_2O/FeSO_4$ and H_2O were manipulated from 60-120 °C, 200-1,000 kmol/h and 1,000-2,000 kmol/h, respectively, to test its effect on the block's calculated heat duty (QCALC). RSTOIC reactor outlet temperature and fractional conversion of $FeSO_4$ were the two manipulated variables analyzed using Aspen Plus for the block. It was found that the reactor QCALC is sensitive to change in $FeSO_4$ fractional conversion (0-1) and the reactor exit temperature from 200-1,000 °C. Next, it was found that the REQUIL-A & B heat duties, vapor fraction and the H_2SO_4 component mass flow out are sensitive to changes in the molar extent. Essentially, molar extent was varied from 0.1-1.0 and 0-2 × 10^{-5} kmol/h in REQUIL-A and REQUIL-B, respectively. At the same time, only vapor fractions and heat duties were found to be sensitive to changes in the temperatures (i.e., 50-500 °C) in the two equilibrium reactors.

3. Results and discussion

3.1 *Process flow diagram*

The result of the successful material flow and unit specifications, resulted in a thoughtfully formulated process flow diagram shown in Figure 1. The design judiciously used 11 blocks consisting of 3 RYield, 1 RStoic and 2 REquil reactors, as well as 1 mixer and 4 separators. It consists of 2 raw materials as feed (i.e., green vitriol and oxygen). Green vitriol of various purity levels can be sourced from chemical suppliers, fertilizer stores, pharmacies, online retailers and hardware stores.

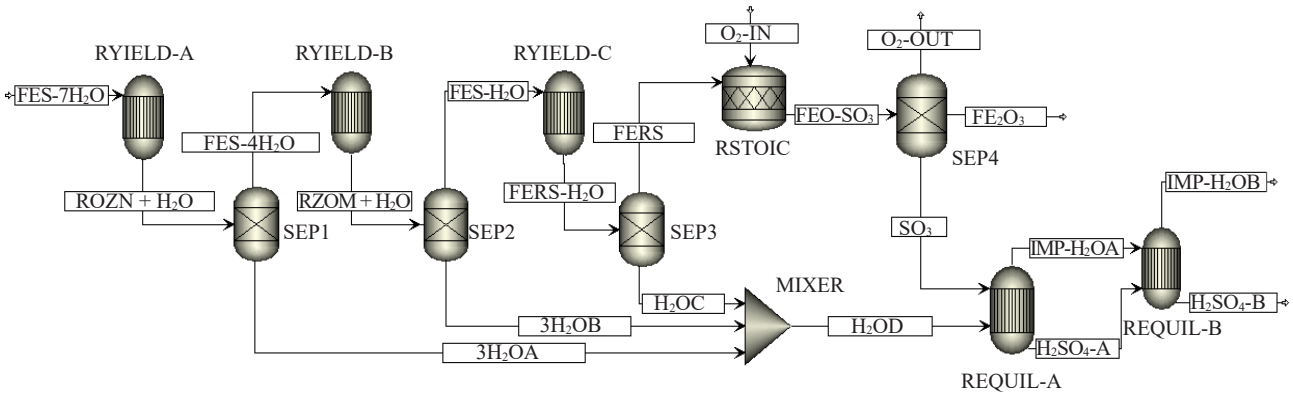

Figure 1. Sulphuric acid synthesis process flow diagram based on Geber's method

The role of the first 3 separators is to remove the water of crystallization contained in the different forms of $FeSO_4$ fed or generated. Since H_2O is needed to form the desired product, it is mixed and re-channeled to an REquil reactor, as a way of conserving material resources. In this simulation, 4 outlet streams of O_2-$FeSO_4$, wastewater, Fe_2O_3 and H_2SO_4 were generated. The wastewater stream still contains unreacted traces of SO_3 and < 1% H_2SO_4, which is > 99% H_2O byproduct. In a report by Mohamed,[15] it is mentioned that H_2SO_4 in water separates to form hydrogen ions (H^+)

and sulfate (SO_4^{2-}). At this point, the synthesized product can be recovered, as clearly illustrated in Figure 2 block flow diagram.

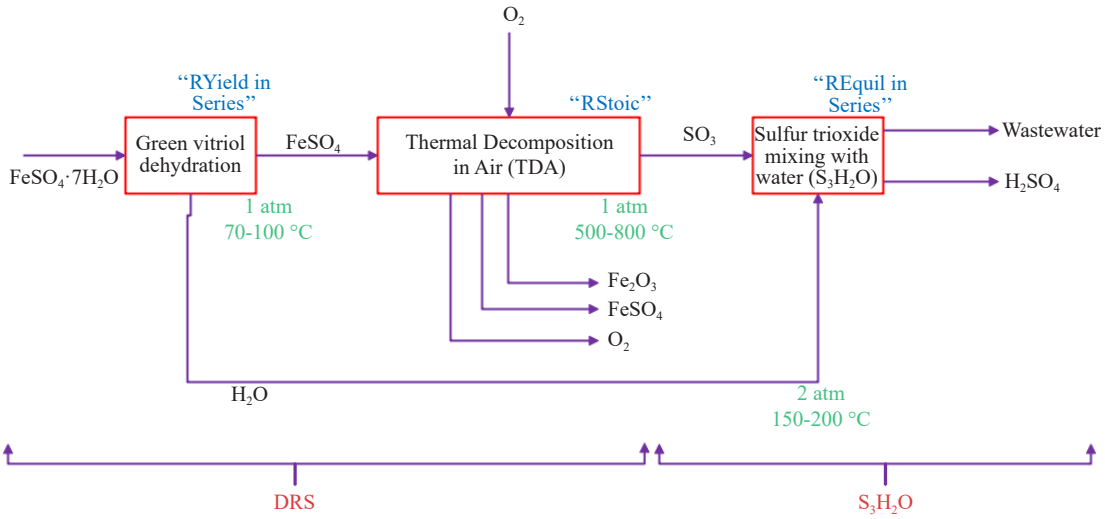

Figure 2. Simplified block flow diagram of H_2SO_4 synthesis based on Geber's method

Because there isn't any harmful gas released into the atmosphere, this design proved the assertion of Mousavi that Geber's method is a harmful gas emission-free H_2SO_4 manufacturing process.[38] Since this study doesn't anticipate any possible wastewater release to the environment, more units may be added to purify or separate the constituents of the IMP-H_2OB stream. Additionally, Muhajir et al. reviewed several other applications of Fe_2O_3 byproduct, making its recovery a useful resource.[39] By the Reaction 7 pathway,[40] Fe_2O_3 can be smelted with carbon to produce iron (Fe).

$$2Fe_2O_{3\,(s)} + 3C_{(s)} \rightarrow 4Fe_{(l)} + 3CO_{2\,(g)} \quad (7)$$

However, a CO_2 atmospheric pollutant would be released. This procedure can be an alternative route to manufacturing CO_2 and/or Fe.

3.2 *Material balance and stream condition*

The high vapor fraction (65.0694%) of the 'FEO + SO_3' stream suggests that the stream is at a temperature and pressure where SO_3 and O_2 are predominantly in the gaseous phase. Iron (III) oxide, being a solid, does not contribute to the liquid fraction but is carried along in the gaseous stream or settles as a solid. Simple reasoning shows that SO_3 has a relatively low boiling point (44.75 °C) and under typical reaction conditions (high temperature around 500-800 °C), it remains in the vapor phase. Similarly, O_2, with its very low boiling point (-182.96 °C), will also be in the vapor phase under these conditions. The presence of a liquid fraction could be due to condensation of any remaining water vapor or minor components that condense at the given temperature and pressure. In Table 3, given that the 'O_2-OUT' stream contains only O_2 and $FeSO_4$, the high liquid fraction (81.201%) is likely due to the presence of $FeSO_4$, which can exist in a hydrated form or as a solid depending on the conditions. Iron (II) sulfate has a much higher boiling point and lower vapor pressure than O_2, causing it to predominantly remain in the liquid (or possibly solid) phase under typical process conditions. Again, the low vapor fraction (18.799%) in this stream is primarily O_2, which remains in the gaseous phase due to its very low boiling point (-182.96 °C). Therefore, the liquid fraction represents $FeSO_4$, which does not easily vaporize under the operational conditions. This behavior indicates that while O_2 remains gaseous, the $FeSO_4$ is not in a vapor state, leading to the observed liquid (or solid) phase fraction in the 'O_2-OUT' stream.

Table 3. Stream condition computations summary

Metric	Stream									
	$FES\text{-}7H_2O$	$ROZN + H_2O$	$3H_2OA$	$FES\text{-}4H_2O$	$SZOM + H_2O$	$3H_2OB$	$FES\text{-}H_2O$	$FERS + H_2O$	H_2OC	FERS
Temp. (°C)	25	70	70	70	70	70	70	70	70	70
Pressure (atm)	1	1	1	1	1	1	1	1	1	1
Vapor frac.	0	0	0	0	0	0	0	0	0	0
Liquid frac.	1	1	1	1	1	1	1	1	1	1
Solid frac.	0	0	0	0	0	0	0	0	0	0
Enthalpy (cal/g)	-2,621.21	-2,584.79	-3,743.77	-2,305.12	-2,263.48	-3,743.77	-1,792.67	-1,033.57	-3,743.77	-712.165
Enthalpy (cal/mol)	-728,740	-179,650	-67,445.1	-516,280	-126,740	-674,45.1	-304,620	-87,815.2	-67,445.1	-108,190
Enthalpy (kcal/h)	-262,120	-258,480	-72,777.9	-185,700	-182,350	-72,777.9	-109,570	-63,172.4	-24,259.3	-38,913.1
Entropy (cal/g·K)	-7.49495	-5.29791	-2.02202	-6.10834	-3.40668	-2.02202	-3.87336	1.33579	-2.02202	1.71587
Entropy (cal/mol·K)	-2,083.73	-368.228	-36.4273	-1,368.1	-190.75	-36.4273	-658.185	113.493	-36.4273	260.659
Density (g/cm^3)	2.11056	1.44495	0.949417	1.58614	1.16406	0.949417	1.20339	1.09404	0.949417	1.07581
Density (mol/cm^3)	0.00759	0.02079	0.05270	0.00708	0.02079	0.05270	0.00708	0.01288	0.05270	0.00708
Average MW	278.018	69.5044	18.0153	223.972	55.9929	18.0153	169.926	84.9629	18.0153	151.911
	Component mass flow (kg/h)									
$FeSO_4$	-	-	-	-	-	-	-	54.64065	-	54.64065
$FeSO_4·H_2O$	-	-	-	-	61.12056	-	61.12056	-	-	-
$FeSO_4·4H_2O$	-	80.56028	-	80.56028	-	-	-	-	-	-
$FeSO_4·7H_2O$	100	-	-	-	-	-	-	-	-	-
H_2O	-	19.43972	19.43972	-	19.43972	19.43972	-	6.479907	6.479907	-
SO_3	-	-	-	-	-	-	-	-	-	-
O_2	-	-	-	-	-	-	-	-	-	-
H_2SO_4	-	-	-	-	-	-	-	-	-	-
Fe_2O_3	-	-	-	-	-	-	-	-	-	-
Total flow (kmol/h)	0.35969	1.43876	1.07907	0.35969	1.43876	1.07907	0.35969	0.71938	0.35969	0.35969
Total flow (kg/h)	100	100	19.4397	80.5603	80.5603	19.4397	61.1206	61.1206	6.47991	54.6407
Total flow (L/h)	47.3808	69.2066	20.4754	50.7902	69.2066	20.4754	50.7902	55.8671	6.82514	50.7902

Table 3. (cont.)

Metric	Stream									
	O_2-IN	FEO + SO_3	O_2-OUT	FE_2O_3	H_2OD	SO_3	IMP-H_2OA	H_2SO_4-A	IMP-H_2OB	H_2SO_4-B
Temp. (°C)	600	600	600	600	70	600	150	150	150	150
Pressure (atm)	1	1	1	1	1	1	2	2	2	2
Vapor frac.	1	0.650694	0.18799	0	0	1	1	0	1	0
Liquid frac.	0	0.349306	0.81201	1	1	0	0	1	0	1
Solid frac.	0	0	0	0	0	0	0	0	0	0
Enthalpy (cal/g)	136.708	-1,100.53	-521.691	-1,180.74	-3,743.77	-1,068.53	-3,143.58	-2,114.03	-3,143.63	-2,114.03
Enthalpy (cal/mol)	4,374.5	-118,150	-67,481.1	-188,560	-67,445.1	-85,551.3	-56,837.5	-135,200	-56,837.3	-135,200
Enthalpy (kcal/h)	392.216	-63,291.2	-1,195.88	-32,554.2	-169,820	-29,541	-109,060	-80,995	-109,060	-80,997.9
Entropy (cal/g·K)	0.25178	-0.781823	1.95878	-1.75317	-2.02202	-0.04537	-0.50756	-0.90235	-0.50758	-0.90235
Entropy (cal/mol·K)	8.05657	-83.9359	253.37	-279.967	-36.4273	-3.63221	-9.17698	-57.7104	-9.17709	-57.7103
Density (g/cm^3)	0.00045	0.00230	0.00939	0.57071	0.94942	0.00112	0.00104	1.33216	0.00104	1.33216
Density (mol/cm^3)	1.396E-05	2.141E-05	7.261E-5	0.00357	0.05270	1.396E-05	5.76E-5	0.02083	5.76E-5	0.02083
Average MW	31.9988	107.359	129.351	159.692	18.0153	80.0642	18.0805	63.9558	18.0801	63.9556
	Component mass flow (kg/h)									
$FeSO_4$	-	2.18563	2.18563	-	-	-	-	-	-	-
$FeSO_4·H_2O$	-	-	-	-	-	-	-	-	-	-
$FeSO_4·4H_2O$	-	-	-	-	-	-	-	-	-	-
$FeSO_4·7H_2O$	-	-	-	-	-	-	-	-	-	-
H_2O	-	-	-	-	45.3594	-	34.5394	4.59966	34.5388	4.59986
SO_3	-	27.6463	-	-	-	27.6463	0.000933	2.25×10^{-5}	6.98×10^{-9}	1.68×10^{-10}
O_2	2.869	0.106688	0.106688	-	-	-	-	-	-	-
H_2SO_4	-	-	-	-	-	-	0.152429	33.7134	0.152426	33.7146
Fe_2O_3	-	27.571	-	27.571	-	-	-	-	-	-
Total flow (kmol/h)	0.08966	0.53568	0.01772	0.17265	2.51783	0.34530	1.91878	0.59906	1.91875	0.59908
Total flow (kg/h)	2.869	57.5097	2.29231	27.571	45.3594	27.6463	34.6926	38.3131	34.6912	39.3145
Total flow (L/h)	6,423.86	25,024.5	244.053	48.3101	47.776	24,739.9	33,312	28.7601	33,311.4	28.7611

The stream at 25 °C is an initial feed condition, representing the ambient temperature before any heating process. Streams at 70 °C are common and represent the intermediate process temperatures where various reactions and separations occur. Temperature of 150 °C is applied to certain streams showcased in Table 3, indicating a stage where higher temperatures are needed for specific reactions or to maintain the solubility and flow properties of certain chemicals. Finally, the temperature of 600 °C was used for high-temperature processes, such as thermal decomposition or reactions requiring elevated temperatures for efficient conversion, including the decomposition of $FeSO_4$ to produce SO_3 and Fe_2O_3.

Enthalpy values in Table 3 indicate the energy changes associated with various streams in the H_2SO_4 synthesis process. The enthalpy values are expressed in different units, including cal/g, cal/mol, and kcal/h, showing the energy content or requirement for each stream. The negative enthalpy values generally suggest exothermic processes, where heat is released. For instance, the stream 'FES-7H_2O' has an enthalpy of -262,120 kcal/h, indicating a significant release of energy. Similarly, 'FES-4H_2O' and 'FES-H_2O' have enthalpy values of -185,700 kcal/h and -109,570 kcal/h, respectively, further pointing towards exothermic reactions. However, streams like 'FES-7H_2O' and 'ROZN + H_2O' show lower enthalpy changes, implying lesser energy exchanges. These enthalpy values highlight that the H_2SO_4 synthesis process involves several exothermic reactions, particularly during the decomposition and hydration stages. The significant release of energy in some streams suggests that the process might be energy-efficient,[41] as the heat generated can potentially be harnessed for other process requirements, reducing the need for external energy input. Entropy values, expressed in cal/g·K and cal/mol·K, vary significantly across different streams, reflecting the complexity and nature of the materials involved. For example, the stream 'ROZN + H_2O' shows an entropy value of -5.29791 cal/g·K, indicating a decrease in disorder. In contrast, the stream 'O_2-OUT' has a high entropy of 1.95878 cal/g·K, suggesting greater molecular randomness. The negative entropy values for many streams such as 'SZOM + H_2O' (-3.40668 cal/g·K) and 'FES-H_2O' (-3.87336 cal/g·K) imply that these processes are associated with a reduction in entropy,[42] which typically corresponds to exothermic reactions where heat is released, leading to more ordered states. Processes with lower entropy changes are often more efficient as they indicate less energy dispersion.[43-44] The negative entropy changes in several streams highlight that the H_2SO_4 synthesis process is designed to be energy-efficient, with significant exothermic reactions contributing to the overall thermodynamic favorability of the process.[45]

Knowing the density and average MW of each stream in a chemical process, such as H_2SO_4 synthesis, is crucial for several reasons. These properties are essential for process design and equipment sizing. Density affects the design of pumps, pipes, and reactors, as higher-density streams (viz., FES-7H_2O, FES-4H_2O, SZOM + H_2O & FES-H_2O, reported in Table 3) require more robust equipment. Average MW is vital for calculating molar flow rates and reaction stoichiometry, ensuring accurate reactor design and proper reactant proportions. These properties are also critical for performing material and energy balances, which are fundamental for process optimization-by ensuring that all input and output streams are correctly accounted for. Density influences volumetric flow rates,[46] affecting the residence time and the design of separators and other equipment. There is a visible deviation from the balanced scheme (mass flow basis: 102.869 kg/h total feed ≠ 103.869 kg/h total product) for the overall process, which could be sorted out using correct component feed amount specifications. This makes Table 3 a converged simulation result with moderate warnings by Aspen Plus, including: Specified yields have been normalized by a factor of (99,984.6) for RYIELD-A; Specified yields have been normalized by a factor of (80,586.1) for RYIELD-B and; Specified yields have been normalized by a factor of (61,130.0) for RYIELD-C, to maintain an overall material balance. Thus, the convergence depicts a feasible process, as the warnings only point to corrections made by the software used.

3.3 *Variation in responses*

Heat duties of the participating reactors shown in Table 4 are sensitive to changes in the specific reactor input parameters.

According to the Aspen Plus report, the heat duties estimated are equal to the net heat duty.

Table 4. Reactors heat duties

Block	Heat duty (kcal/h)
RYIELD-A	3,641.83
RYIELD-B	3,353.98
RYIELD-C	46,396.4
RSTOIC	-24,770.2
REQUIL-A	9,302.37
REQUIL-B	-0.545284

3.3.1 *RYIELD blocks*

Repeated sensitivity tests show that only heat duty is sensitive to changes in the component mole yield and block temperature, as shown in Figures 3 and 4. Figure 3a illustrates the effect of unit temperature on heat duty for RYIELD-A and RYIELD-B units following a sensitivity analysis. As temperature increases from 55-105 °C, both units exhibit a gradual, nearly linear rise in heat duty, indicating low sensitivity to temperature changes in this range. However, beyond 105 °C, a sharp increase in heat duty is observed, reflecting a high sensitivity likely due to phase changes or chemical reactions requiring significantly more heat.

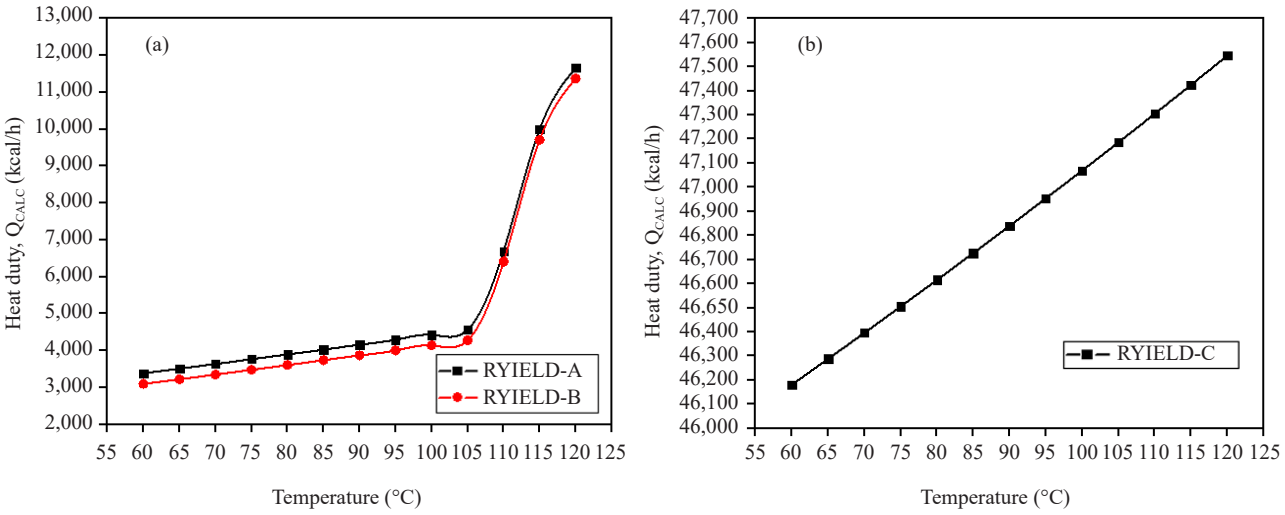

Figure 3. Effect of unit temperature on heat duty, (a) for RYIELD-A and RYIELD-B units, (b) for RYIELD-C

RYIELD-B shows slightly lower heat duty than RYIELD-A below 115 °C, suggesting marginally higher efficiency, but both units converge in performance at higher temperatures. Figure 3a highlights the importance of precise temperature control and consideration of increased energy requirements for operations exceeding 105 °C to ensure efficient and stable unit operation. In contrast, RYIELD-C shows a consistent, linear increase in heat duty across the entire temperature range, with significantly higher overall heat duty starting around 46,000 kcal/h and rising to 47,700 kcal/h (Figure 3b). This linear response simplifies thermal management but comes with higher energy consumption compared to RYIELD-A and RYIELD-B, which are more efficient at lower temperatures but require careful control at higher temperatures due to their non-linear heat duty increase. Figure 4a compares QCALC and mole yield of three

different compounds, $FeSO_4 \cdot 4H_2O$, $FeSO_4 \cdot H_2O$, and $FeSO_4$, for the RYIELD-A, RYIELD-B, and RYIELD-C units, respectively.

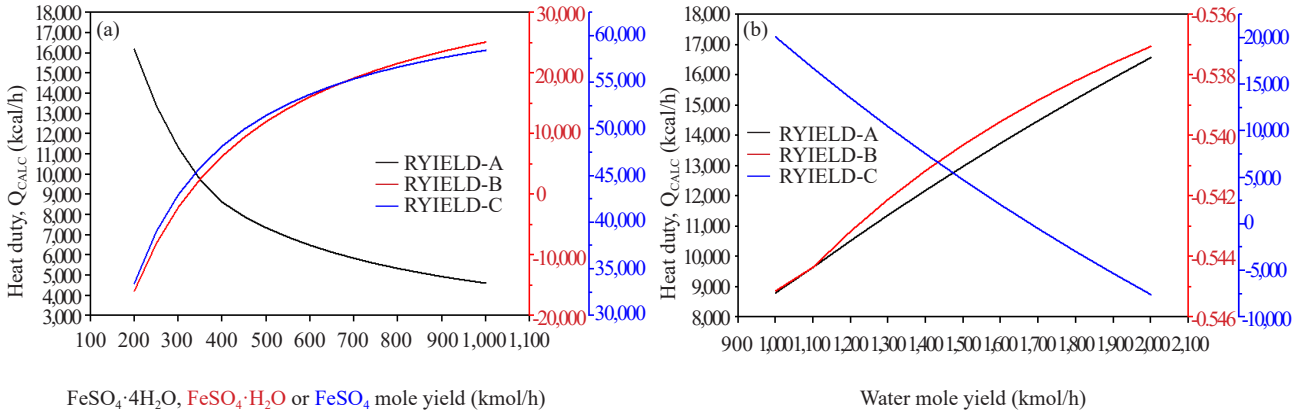

Figure 4. Effect of reactant component mole yield on heat duty, $FeSO_4 \cdot 4H_2O$, $FeSO_4 \cdot H_2O$, and $FeSO_4$ (a); water (b)

RYIELD-A (Figure 4a) shows a significant decrease in heat duty as mole yield increases, indicating high efficiency but achieving lower maximum yields. RYIELD-B and RYIELD-C both exhibit a steady incline in heat duty with yield, with RYIELD-B being slightly more efficient than RYIELD-C. However, RYIELD-C achieves the highest overall yields. Thus, RYIELD-A offers lower yields with better energy efficiency, while RYIELD-B and RYIELD-C offer a higher yield despite their higher energy consumption. Figure 4b is in terms of water mole yields, where RYIELD-A and RYIELD-B duty peaked with water yield, but RYIELD-C heat duty declined.

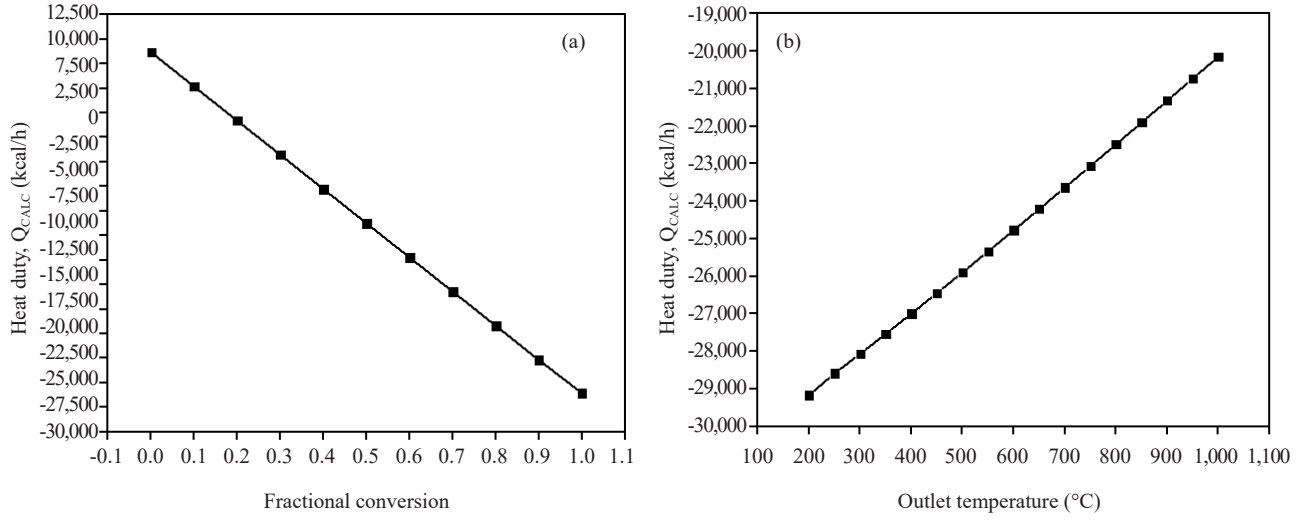

Figure 5. RSTOIC response variable values, (a) for fractional conversion of $FeSO_4$ and (b) for temperture

3.3.2 *RSTOIC unit*

It was found that the heat duty of the RSTOIC reactor is sensitive to variations in the outlet temperature and

fractional conversion of $FeSO_4$, as illustrated in Figure 5. In Figure 5a, it was observed that heat duty decreases as the fractional conversion of $FeSO_4$ increases from 0-1. This trend is primarily due to the exothermic nature of the reaction, where increased conversion releases more heat, thereby reducing the need for external heat input. As more $FeSO_4$ is converted into products, the system utilizes the released heat more effectively, improving thermodynamic efficiency and decreasing the external heat duty required to maintain the reactor's temperature. This leads to a more self-sustaining reaction process at higher fractional conversions, especially at 0.96 specified during this simulation.

Whereas in Figure 5b, the sensitivity analysis conducted for the RSTOIC process reveals insightful trends between outlet temperature and heat duty, crucial for optimizing operational efficiency. The data demonstrates that as the outlet temperature increases from 200-1,000 °C, the heat duty-indicative of the cooling requirement-consistently increases (i.e., from -29,157 to -20,147 kcal/h). This positive trend indicates that higher outlet temperatures necessitate greater heat removal or cooling within the process. Specifically, the magnitude of heat duty becomes more negative as the outlet temperature rises, highlighting an escalating demand for cooling as temperatures increase.

3.3.3 *REQUIL blocks*

A decreasing trend of heat duty with 'ξ' in Figure 6a, is attributed to the increasing efficiency of the reaction as more reactants are converted into products. As ξ increases from 0.1-1.0 kmol/h, the reaction becomes more exothermic, leading to a higher heat release from the reaction itself. This increased heat generation reduces the external heat input required to sustain the reaction, resulting in a decrease in the overall heat duty. Still, the observation that the vapor fraction becomes constant (i.e., 0.765) in Figure 6a beyond an ξ of 0.4 kmol/h indicates a phase equilibrium or saturation point in the system, corresponding to QCALC = 9,460 kcal/h.

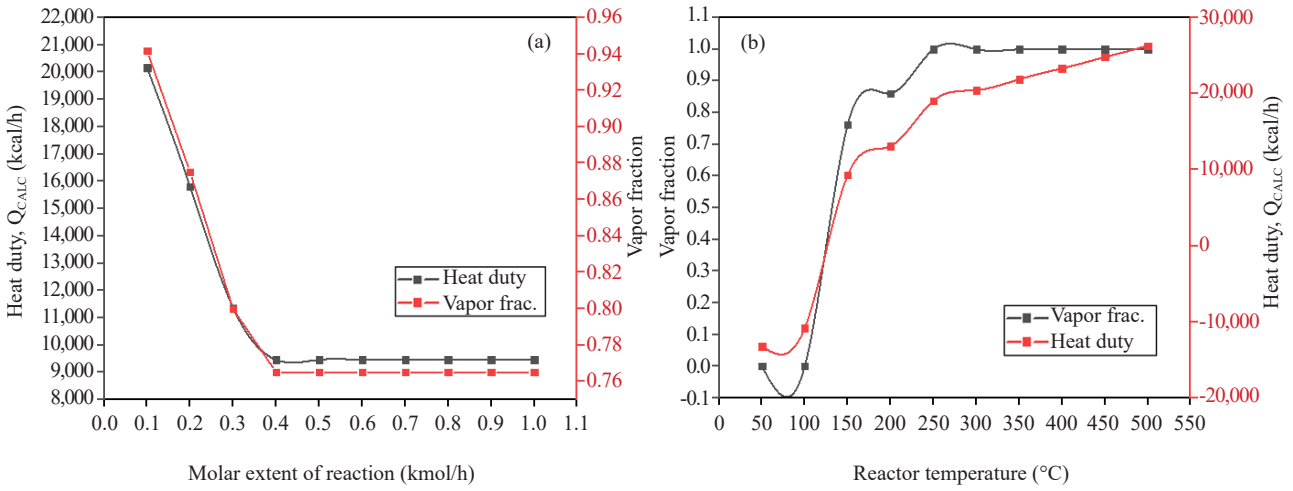

Figure 6. Measured variables response trends for REQUIL-A unit

As the temperature of the REQUIL-A reactor is raised, as shown in Figure 6b, the energy available for vaporization also increases (to 26,301 kcal/h), leading to a higher vapor fraction in the system and the conversion of liquid H_2O components into the vapor phase. The same explanation can be given to Figure 7, showcasing similar trend.

Obviously, the effectiveness of REQUIL-A reactor led to a lower extent specification in REQUIL-B (Figure 7a) in order to further maximize SO_3 conversion to H_2SO_4 and its reduction in the wastewater stream. Figures 7 and 8 show that the REquil reactor is operating at optimal conditions: that is, minimum or maximum heat duty and maximum vapor fraction requirements with ξ and reactor temperature variations, respectively.

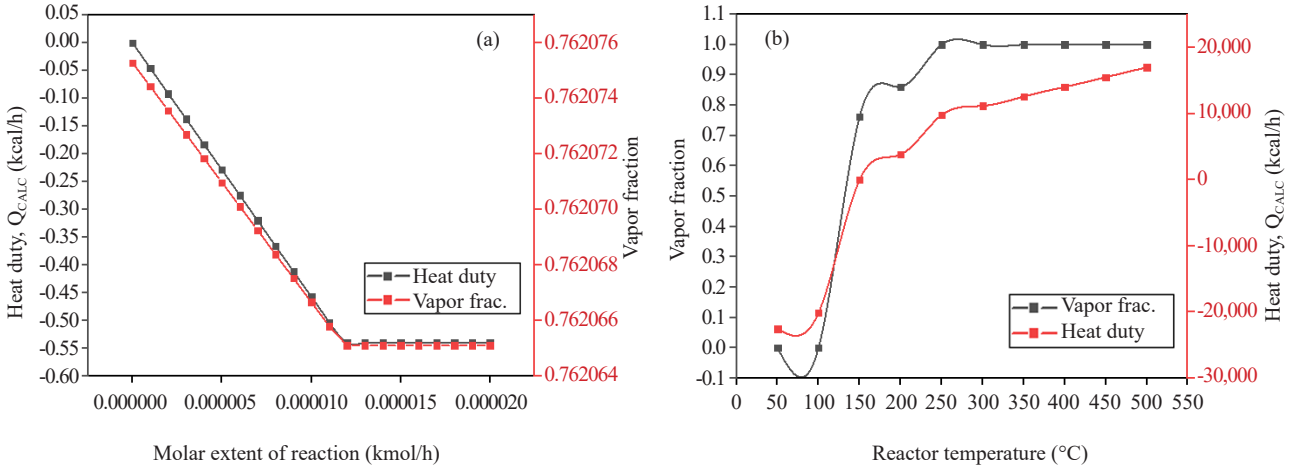

Figure 7. Measured variables response trends for REQUIL-B unit

3.3.4 *Mass flow of sulfuric acid*

Sulfuric acid was generated in stream 'H_2SO_4-A' and 'H_2SO_4-B' as products of REQUIL-A and REQUIL-B, respectively. According to Figure 8a, as ξ_{REq1} increases from 0.1-0.4 kmol/h, there is a significant increase in the mass flow rate of H_2SO_4, from approximately 9.59 kg/h at ξ_{REq1} = 0.1 to about 33.37 kg/h at ξ_{REq1} = 0.4 kmol/h. But once the reaction reaches a certain extent ($\xi_{REq1} \geq 0.4$ kmol/h), the production rate of H_2SO_4 does not increase further with additional reaction progress.

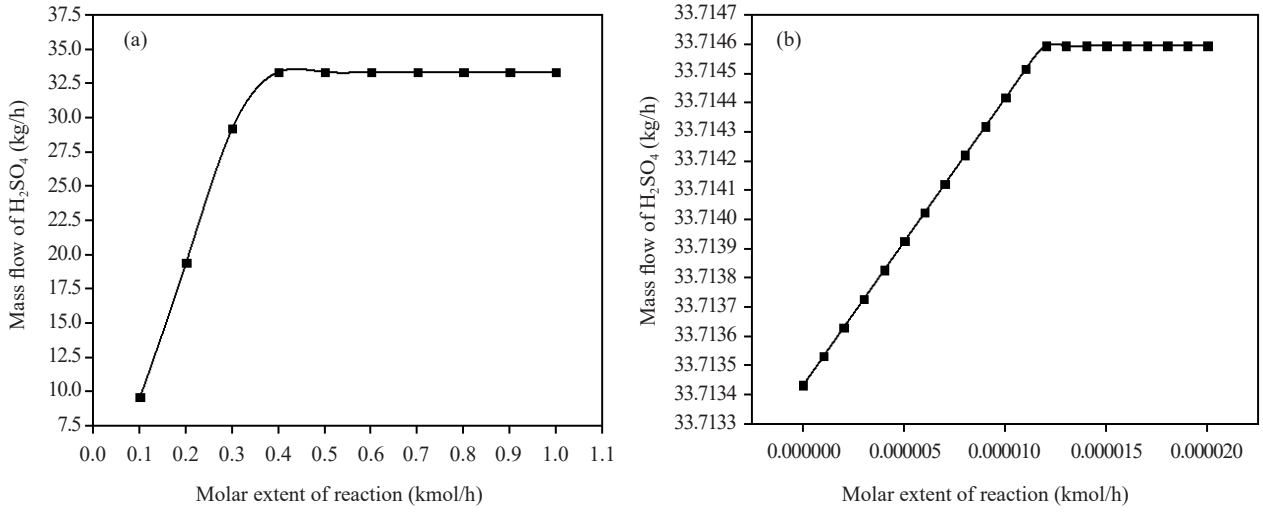

Figure 8. Sulphuric acid maximization in (a) REQUIL-A and (b) REQUIL-B

From an operational perspective, maintaining the reaction at an extent around ξ_{REq1} = 0.4 kmol/h is optimal to maximize H_2SO_4 production efficiently. Beyond this point, increasing the extent of reaction does not result in increased product yield, implying that resources could be better utilized elsewhere in the process. REQUIL-B showcased similar behavior in Figure 8b, presenting an optimum of $\xi_{REq2} = 1.2 \times 10^{-5}$ kmol/h, corresponding to 33.7146 kg/h of H_2SO_4. It shows that a continuous deployment of the REquil reactors in series, just as illustrated in Figure 1 or 2, will continuously

increase the amount of H_2SO_4 recovered. Therefore, 85.76% pure H_2SO_4 is produced from the simulation of the Geber's method in Aspen Plus. However, the H_2SO_4 purity obtained herein is less than those reported for contact processes. The synthesis method is toxic gas emission-free, offering byproducts such as Fe_2O_3, $FeSO_4$ and O_2 which can be recycled further or recovered for different purposes. Other uses of $FeSO_4$ are clearly stated in SIGMA[47] and Yang.[48]

4. Conclusion

In this simulation, green synthesis of H_2SO_4 was achieved using Aspen Plus V8.8, using a simplified process based on the Geber's method, where no greenhouse gas emissions were recorded. The synthesis was divided into DRS and S_3H_2O steps, involving a series of reactors and separators. The selection of an appropriate block or unit for the operation was based on their unique properties and the specific needs addressed within the simulation. The heat duties of the reactors are sensitive to specific input parameters, as several sensitivity analyses have confirmed. The improvement of H_2SO_4 yield was found to be dependent on the molar extent of reaction specified in the REquil reactors arranged in series. As a result, an optimum production of 33.71 kg/h H_2SO_4 (85.76% pure) was obtained using 100 kg/h $FeSO_4{\cdot}7H_2O$ and 2.869 kg/h O_2 as feedstock. Although air pollution is avoided, the wastewater released via the IMP-H_2OB stream contains trace amounts of H_2SO_4 (0.4393%) and SO_3 (2.01298×10^{-8} wt.%), which still makes it harmful to aquatic habitats and for consumption purposes. Since $FeSO_4$ and O_2 are useful byproducts of the synthesis, they can be recycled or preferably recovered for several applications. Additional units to purify the wastewater stream containing trace concentration of the acid should be integrated, and the recovered separated streams recycled back to the system. This study validates the Geber's method as an energy efficient and nearly pollution-free method of manufacturing H_2SO_4, whose adoption was previously recommended by concerned researchers.

Acknowledgments

The authors are grateful to the members of staff of the respective institution, for their useful contributions. The authors specially expressed their thanks to Prof. Ronny Monning and Engr. Lukman Buba Umdagas for assisting in the review of this work. We acknowledge the valuable suggestions from the peer reviewers.

Conflict of interest

The authors declare no competing interest attributed to this work.

References

[1] Garcia-Labiano, F.; De Diego, L. F.; Cabello, A.; Gayan, P.; Abad, A.; Adanez, J.; Sprachmann, G. Sulphuric acid production via chemical looping combustion of elemental sulphur. *Appl. Energy* **2016,** *178*, 736-745.
[2] Mousavi, A. "Geber's method" and "Greener" synthesis of sulfuric acid. *J. Mater. Environ. Sci*. **2012,** *3*(2), 391-394.
[3] Kragh, H. *Sulphuric Acid was the Bedrock of the Industrial Revolution*; ScienceNordic, 2017. https://www.sciencenordic.com/chemistry-denmark-researcher-zone (accessed April 5, 2024).
[4] Karpenko, V.; Norris, J. A. Vitriol in the history of chemistry. *Chem. List*. **2002,** *96*(12), 997-1005.
[5] Hanekom, J. Sulphuric acid plant optimization and troubleshooting. *J. S. Afr. Inst. Min. Metall*. **2017,** *117*, 1031-1034.
[6] Mperiju, T.; Sylvain, T.; Arowo, M. N.; Dhanda, T.; Abubakar, A. M.; Goriya, B. A.; Abdul, A. Z. Optimized production of high purity sulphuric acid via contact process. *Logist. Oper. Manag. Res.* **2023,** *2*(1), 1-13.
[7] Infoplease. Sulfuric acid: history of sulfuric acid. In *The Columbia Electronic Encyclopedia*; Columbia University Press, 2024.
[8] Sultana, S. T.; Amin, M. R. Aspen-Hysys simulation of sulfuric acid plant. *J. Chem. Eng*. **2011,** *26*(1), 47-49.

[9] Seo, D.; Hong, S. D.; Kim, C. S.; Kim, J. H.; Kim, Y. W.; Chang, J. H.; Park, G. C. In *Modeling of a High Temperature Sulfuric Acid Loop Using Aspen Plus*, Transactions of the Korean Nuclear Society Autumn Meeting; Gyeongju, Korea, 2009; pp 107-108.
[10] Richardson, S.; Trapet, A.; Brouwers, T. How to effectively manage and reduce emissions in sulfuric acid plants using state-of-the-art MECS® catalysts. *Procedia Eng.* **2016,** *138*, 199-205.
[11] Mohammed, M. M.; Barbuti, M. M.; Rashid, R. S.; Muneer, H. K. Removal of sulfur dioxide from sulfuric plant emissions. *Iraqi J. Chem. Pet. Eng*. **2002,** *3*, 31-34.
[12] Saleh, M. A.; Fayed, M. S.; El-Rifai, M. A. Air pollution in a sulphuric acid plant. In *Environmental Engineering*; Lindner, G., Nyberg, K., Eds.; Springer: Dordrecht, 1973; pp 105-112.
[13] Worley. *Installing Sustainable Sulphuric Acid Technology for Arafura*; 2023. https://www.worley.com/en/insights/our-news/digital-and-technology/2023/ (accessed April 19, 2024).
[14] Lemessa, A.; Birlie, M.; Kassahun, M.; Mengistu, Y. In *Process revamping of H_2SO_4 plant to double contact double absorption (DCDA) using ASPEN HYSYS to reduce SO_2 emission: Case of awash melkassa sulfuric acid factory*, International Conference on Advances of Science and Technology; Berihun, M. L., Ed.; Cham: Springer, 2022; pp 59-72.
[15] Mohamed, F. *Environmental Impact of Chemical Industry Air Pollutants (Sulfuric Acid Production)*; 2022.
[16] Tsiura, N.; Kindzera, D.; Huzova, I.; Atamanyuk, V. Study of the kinetics of drying iron (II) sulfate heptahydrate by filtration method. *ScienceRise* **2021,** *1*, 11-21.
[17] Cameron, F. K. The solubility of ferrous sulphate. *J. Phys. Chem*. **1930,** *34*(4), 692-710.
[18] Zhang, S.; Shi, R.; Huang, H. Comparison of the solubility of $ZnFe_2O_4$, Fe_3O_4 and Fe_2O_3 in high temperature water. *J. Solution Chem*. **2018,** *47*(6), 1112-1126.
[19] Daub, C. D.; Riccardi, E.; Hanninen, V.; Halonen, L. Path sampling for atmospheric reactions: Formic acid catalysed conversion of SO_3 + H_2O to H_2SO_4. *PeerJ Phys. Chem*. **2020,** *2*(e7), 1-15.
[20] Akhmatskaya, E. V; Apps, C. J.; Hillier, I. H.; Masters, A. J.; Watt, N. E.; Whitehead, J. C. Formation of H_2SO_4 from SO_3 and H_2O, catalysed in water clusters. *Chem. Commun*. **1997,** *7*, 707-708.
[21] Vetere, A. The NRTL equation as a predictive tool for vapor-liquid equilibria. *Fluid Phase Equilib*. **2004,** *218*(1), 33-39.
[22] Labarta, J. A.; Olaya, M. M.; Marcilla, A. F. What does the NRTL model look like? Determination of boundaries for different fluid phase equilibrium regions. *AIChE J*. **2022,** *68*(10), e17805.
[23] De Tommaso, J.; Rossi, F.; Kazerooni, N. M.; Pirola, C.; Patience, G. S.; Galli, F. Experimental methods in chemical engineering: Process simulation. *Can. J. Chem. Eng*. **2020,** *98*, 2301-2320.
[24] Wang, T.; Debelak, K. A.; Roth, J. A. Dehydration of Iron(II) sulfate heptahydrate. *Thermochim. Acta* **2007,** *462*(1-2), 89-93.
[25] Sutherland, G.; Mitchell, A. G. The dehydration and hydration of ferrous sulphate. *J. Pharm. Pharmacol*. **1982,** *34*(12), 9.
[26] Kanari, N.; Menad, N.-E.; Ostrosi, E.; Shallari, S.; Diot, F.; Allain, E.; Yvon, J. Thermal behaviour of hydrated iron sulfate in various atmospheres. *Metals (Basel)* **2018,** *8*(1084), 1-9.
[27] Hongbo, M.; Tianzhu, M.; Bin, D.; Sanchao, Z.; Beilei, Y.; Fuxing, Z.; Weixing, P. Method for Removing Crystal Water in Green Vitriol. CN104045118A, 2015. https://patents.google.com/patent/CN104045118A/en (accessed April 19, 2024).
[28] Kobylin, P. M.; Sippola, H.; Taskinen, P. A. Thermodynamic modelling of aqueous Fe(II) sulfate solutions. *Calphad* **2011,** *35*, 499-511.
[29] Gallagher, P. K.; Johnson, D. W.; Schrey, F. Thermal decomposition of Iron(II) sulfates. *J. Am. Ceram. Soc*. **2006,** *53*(12), 666-670.
[30] Kamel, A. H.; Sawires, Z.; Khalifa, H.; Saleh, S. A.; Abdallah, A. M. The thermal decomposition of ferrous sulphate heptahydrate. I. Dehydration and oxidation. *J. Appl. Chem. Biotechnol*. **1972,** *22*(5), 591-598.
[31] Chaves, I. D. G.; L opez, J. R. G.; Zapata, J. L. G.; Robayo, A. L.; Nino, G. R. *Process Analysis and Simulation in Chemical Engineering*; Springer International Publishing Switzerland, 2016.
[32] Long, B.; Chang, C.-R.; Long, Z.-W.; Wang, Y.-B.; Tan, X.-F.; Zhang, W.-J. Nitric acid catalyzed hydrolysis of SO_3 in the formation of sulfuric acid: A theroretical study. *Chem. Phys. Lett*. **2013,** *581*, 26-29.
[33] Hofmann-Sievert, R.; Castleman, A. W. Reaction of sulfur trioxide with water clusters and the formation of sulfuric acid. *J. Phys. Chem*. **1984,** *88*, 3329-3333.
[34] Hesketh, R. P.; LaMarca, C. *Stoichiometric Reactor Simulation*; Chemical Engineering, Rowan University, 2009. https://www.cartagena99.com/recursos/fisica/apuntes/TUTORIAL 2P3.pdf (accessed May 20, 2024).

[35] Gaspar, V.; Toth, J. Reaction extent or advancement of reaction: A definition for complex chemical reactions. *Chaos* **2023,** *33*(4), 1-97.
[36] Novak, I. Reversible reactions: Extent of reaction and theoretical yield. *J. Chem. Educ*. **2020,** *97*(2), 443-447.
[37] Higgins, B. G. *Reaction Rate and the Extent of Reaction: An Overview*; University of California, Davis, 2022. https://www.researchgate.net/publication/362405484 (accessed May 30, 2024).
[38] Mousavi, A. "Geber's method" in environmental perspective revisited. *Comments Inorg. Chem*. **2015,** *35*(5), 255-261.
[39] Muhajir, M.; Puspitasari, P.; Abdul Razak, J. Synthesis and applications of hematite α-Fe_2O_3: A review. *J. Mech. Eng. Sci. Technol*. **2019,** *3*(2), 52-58.
[40] Dos Santos, D. M.; Mourao, M. High-temperature reduction of iron oxides by solid carbon or carbon dissolved in liquid iron-carbon alloy. *Scand. J. Metall*. **2004,** *33*(4), 229-235.
[41] Jang, W. Exothermic reactions: Its energy release and applications. *J. Adv. Chem. Eng*. **2023,** *13*(2), 277.
[42] Chang, Y.-F. Decrease of Entropy and Chemical Reactions. 2008, arXiv:0807.0256. arXiv.org e-Print archive. https://doi.org/10.48550/arXiv.0807.0256 (accessed June 1, 2024).
[43] Koukkari, P.; Liukkonen, S. S. Calculation of entropy production in process models. *Ind. Eng. Chem. Res*. **2002,** *41*(12), 2931-2940.
[44] Shin, W.; Yang, Z. J. Computational strategies for entropy modeling in chemical processes. *Chem. Asian J*. **2023,** *18*(9), 1-25.
[45] Goupil, C. Entropy. In *Simulation with Entropy Thermodynamics*; Goupil, C., Ed.; MDPI, 2021; pp 222.
[46] Bott, A.-K.; Felber, T.; Kohler, M. Estimation of a density in a simulation model. *J. Nonparametr. Stat*. **2015,** *27*(3), 1-15.
[47] SIGMA. *Iron(II) Sulfate Heptahydrate*; Sigma-Aldrich, Inc: Saint Louis, Missouri, 2004. http://www.sigmaaldrich.com (accessed June 1, 2024).
[48] Yang, K.-J. *Recovery of Ferrous Sulfate Crystals From Pickling Liquor*; California Institute of Technology, 1926. https://core.ac.uk/download/pdf/11809011.pdf (accessed June 9, 2024).